STRUCTURAL DYNAMICS 2, 041712 (2015)

Real-time investigation of dynamic protein crystallization in living cells[a)]

R. Schönherr,[1,b)] M. Klinge,[2,b)] J. M. Rudolph,[1,2] K. Fita,[2] D. Rehders,[2] F. Lübber,[1,2] S. Schneegans,[1,2] I. V. Majoul,[1] M. Duszenko,[3] C. Betzel,[4] A. Brandariz-Nuñez,[5,c)] J. Martinez-Costas,[5] R. Duden,[1] and L. Redecke[2,d)]
[1]*Institute of Biology, Center for Structural and Cell Biology in Medicine, University of Lübeck, Ratzeburger Allee 160, 23562 Lübeck, Germany*
[2]*Institute of Biochemistry, Center for Structural and Cell Biology in Medicine, University of Lübeck, Ratzeburger Allee 160, 23562 Lübeck, Germany*
[3]*Interfaculty Institute of Biochemistry, University of Tübingen, Hoppe-Seyler-Straße 4, 72076 Tübingen, Germany*
[4]*Institute of Biochemistry and Molecular Biology, University of Hamburg, c/o DESY, Notkestr. 85, 22603 Hamburg, Germany*
[5]*Department of Biochemistry and Molecular Biology, Centro de Investigación en Química Biológica y Materiales Moleculares (CIQUS), University Santiago de Compostela, 15782 Santiago de Compostela, Spain*

(Received 27 February 2015; accepted 5 May 2015; published online 22 May 2015)

X-ray crystallography requires sufficiently large crystals to obtain structural insights at atomic resolution, routinely obtained *in vitro* by time-consuming screening. Recently, successful data collection was reported from protein microcrystals grown within living cells using highly brilliant free-electron laser and third-generation synchrotron radiation. Here, we analyzed *in vivo* crystal growth of firefly luciferase and Green Fluorescent Protein-tagged reovirus μNS by live-cell imaging, showing that dimensions of living cells did not limit crystal size. The crystallization process is highly dynamic and occurs in different cellular compartments. *In vivo* protein crystallization offers exciting new possibilities for proteins that do not form crystals *in vitro*. [http://dx.doi.org/10.1063/1.4921591]

I. INTRODUCTION

The three-dimensional structure of a protein determines its function. Consequently, structural insights into proteins at atomic resolution are important to understand the machinery of life or to develop new specifically designed drugs for medical applications. Synchrotron-based x-ray crystallography, the preferred technique for obtaining structural information at high resolution, accounts for almost 90% of the over 107.000 protein structures deposited within the Protein Data Bank (PDB, www.pdb.org) to date. Despite the revolutionary success during the past decades, the correlation between crystal size, diffraction intensity, resolution, and radiation damage usually requires the growth of sufficiently large and well-ordered single crystals and thus emphasizes one of the major bottlenecks of this method.[1,2] The deposited energy triggers a variety of chemical reactions that finally reduce the crystalline order, leading to a quick deterioration of the diffraction data quality as a function of the applied x-ray dose, even under cryogenic conditions.[3,4] Lowering the incident fluency to reduce radiation damage in turn requires

[a)]Contributed paper, published as part of the Proceedings of the 2nd International BioXFEL Conference, Ponce, PR, January 2015.
[a)]R. Schönherr and M. Klinge contributed equally to this work.
[c)]Present address: Department of Biochemistry, Center for Biophysics and Computational Biology, University of Illinois at Urbana-Champaign, Urbana, Illinois 61801, USA.
[d)]Author to whom correspondence should be addressed. Electronic mail: redecke@biochem.uni-luebeck.de

the growth of large crystals to yield sufficient diffraction intensities, which is difficult in many cases, particularly for post-translationally modified proteins and membrane proteins.[5]

Conventional protein crystallization in artificial crystallization chambers requires the promotion of the nucleation process when a supersaturated sample solution is introduced to a precipitating agent *in vitro*. If the environmental conditions fit, the growth of large three-dimensional crystals may result. This process is affected by a wide range of parameters, generating a vast multidimensional space that must be screened to meet the desired conditions yielding crystals. In modern crystallization approaches, pipetting robot-assisted sparse matrix screening approaches are routinely performed to test the potential crystallization space applying vapor diffusion and batch crystallization techniques. Although the success rate has significantly improved to date, there is still no guarantee for protein crystal formation.[6,7]

For more than a century, it has been known that protein crystallization also represents a native, if somewhat rare, process within living cells.[8] Intracellular crystalline states of proteins are associated with diverse cellular functions, as observed for storage proteins in seeds,[9–11] insulin in pancreatic β-cells,[12] enzymes in peroxisomes,[13] and bacterial toxins.[14] Moreover, spontaneous crystal formation *in vivo* may also occur as a result of heterologous gene overexpression. Polyhedrin, a viral protein that usually forms a crystalline coat to protect virions against environmental challenges,[15] assembles into remarkably stable microcrystals within virus-infected insect cells.[16] Exploiting the permanent activation of the polyhedrin promotor, the exchange of the polyhedrin gene by a gene of interest in a baculovirus shuttle vector results in high local protein concentration in the baculovirus-infected insect cell, which is obviously one prerequisite for *in vivo* crystal formation. Thus, protein microcrystals have been discovered several times by applying the well-established baculovirus-Sf9 insect cell expression system that is frequently used to produce recombinant proteins containing post-translational modifications.[17] Mammalian cells also provide a suitable environment for heterologous protein crystallization, as recently demonstrated.[18–20] However, the phenomenon of *in vivo* crystallization was so far largely perceived as a rare and atypical behavior of proteins, preventing a systematic investigation of the intracellular crystallization process. The size of the crystal grown *in vivo* was previously considered to be necessarily limited by the cell's outer dimensions,[8,21] but such small crystals would harbor only low diffraction capabilities and high sensitivity to radiation damage. Thus, *in vivo* grown protein crystals were not considered for structural biology until recently.

This picture has significantly changed with the recent realization of novel radiation sources that produce x-rays of previously inaccessible energy and brilliance. Exploiting the "diffraction-before-destruction" paradigm[22] by using highly brilliant x-ray free-electron laser (XFEL) pulses of a few femtoseconds duration, serial femtosecond crystallography (SFX) has already been shown to overcome resolution limits imposed by radiation damage at conventional synchrotron sources, allowing serial diffraction data collection from unprecedentedly small protein crystals down to the nanometer regime.[23,24] Tens of thousands of Bragg-diffraction snapshots from individual, randomly "oriented" crystals are recorded at room temperature (RT) and then combined into a dataset applying new data-processing tools[25–27] to produce interpretable electron density maps. Since each pulse destroys the individual crystal, samples need to be constantly supplied by injection in vacuum into the pulsed XFEL beam using microjet techniques.[28,29] The feasibility of this concept to elucidate protein structures at high resolution has already been demonstrated on several examples.[23,24,30–34] One of the important milestones in SFX development, namely, the elucidation of the first new bioinformation by applying this approach, has been obtained using protein crystals that spontaneously grew within living baculovirus-infected Sf9 insect cells during gene over-expression.[30] In addition to the applicability of SFX techniques, we recently showed that comparable structural information on fully glycosylated and natively inhibited *Trypanosoma brucei* procathepsin B could be obtained from the same *in vivo* crystals combining a micron-sized synchrotron beam with high-precision diffractometry and a helical line scan approach.[35] Although the resolution of the diffracted synchrotron radiation was slightly reduced, which indicates the need for further methodological and technical improvement. Particularly, optimization of the sample mounting and a more focused X-ray beam are currently in discussion.[35] Both studies clearly illustrated that *in vivo* crystals can indeed act as

suitable targets for structural biology, if the enormous potential of the highly brilliant XFEL and third-generation synchrotron radiation sources is exploited. This significantly supports and extends initial studies reporting the successful structure solution from *in vivo*-produced polyhedra at microfocus synchrotron beamlines.[16,36,37]

The number of *in vivo* crystallization observations reported as a consequence of heterologous gene expression increased within the past years,[18,20,38] but crystal formation within a living cell still represents a spontaneous event that is detected by chance. A broader application of *in vivo* grown protein crystals as valuable targets for structural biology requires a detailed and systematic investigation of the intracellular processes involved in crystal formation. If identified, the modification of suitable biological parameters that influence crystal growth could significantly increase the chance of successful protein crystallization within living cells, comparable to multidimensional parameter screens performed in conventional crystallography. Such biological parameters could include, for example, the localization of the protein in a specific cellular compartment as well as the up or down regulation of distinct cellular pathways impacting on protein degradation or trafficking. In this context, we analysed the spontaneous crystal formation of two proteins in Sf9 insect cells, namely, firefly luciferase and a part of the avian reovirus (ARV) nonstructural protein μNS (residues 448-605) fused to Green Fluorescent Protein (GFP) (referred to as GFP-μNS). Applying live-cell imaging techniques, we obtained first real-time insights into the dynamic crystallization process in a living cell, together with new results in terms of cellular localization, stability, and diffraction capabilities of the *in vivo* grown protein crystals, which are discussed in this study.

II. EXPERIMENTAL METHODS

A. Recombinant baculovirus generation and gene expression

The construction of the recombinant baculoviruses Bac-luc, which expresses full length luciferase from *Photinus pyralis* (American firefly), and Bac-GFP-μNS, which expresses GFP-μNS (448–605) from the avian reovirus S1133 strain, have previously been described.[39,40] For baculovirus–driven expression of mCherry labeled organelle marker proteins, Pex3-mCherry,[41] Pex26-mCherry,[41] and mCherry-KDEL[42] were subcloned into pFastBac1 using EcoRI and XbaI restriction enzymes. The construction of recombinant baculoviruses and subsequent generation of high-titer virus stocks were performed according to the Bac-to-Bac manual (Invitrogen). Recombinant high-titer virus stocks (P3) were used to infect 70%-confluent monolayer cultures of Sf9 insect cells (an insect cell line derived from *Spodoptera frugiperda* (ATCC CRL-1711, Invitrogen) with a multiplicity of infection of 0.1 p.f.u. per cell. Sf9 cells were grown in serum-free EX-CELL 420 insect cell medium (Sigma) supplemented with 100 units/ml penicillin and 100 μg/ml streptomycin at 26 °C.

B. Microscopy and live cell imaging

Transiently transfected or baculovirus infected Sf9 cells were plated on glass coverslips and adherent cells were imaged using a laser confocal spinning disk microscope system based on a Nikon Ti Eclipse microscope equipped with the confocal spinning unit CSU-X1 and an Andor iXon + EM-CCD (electron multiplier-charge coupled device) camera. The microscope was fitted with 40×, 1.30 NA and 100×, 1.49 NA objectives. Image acquisition was controlled with Andor Bioimaging software (Andor IQ2.1). Protein crystal growth and dynamics in living Sf9 cells were recorded by time-lapse microscopy using differential interference contrast (DIC) optics over a period of several days or, in the case of GFP-μNS, using a combination of DIC microscopy and GFP fluorescence that was elicited with a 514 nm laser. For 3D images of living cells, z-stacks were taken with images every 300 nm. Three dimensional reconstruction and animation were done in Andor IQ2.1.

Cells infected with recombinant Bac-luc and Bac-GFP-μNS have been subjected to propidium iodide (PI) staining[43] to detect dead cells in the culture and to BODIPY® 558/568 C_{12} (Life Technologies) treatment for staining of internal cellular membranes. Cells were plated on 25 mm glass coverslips at 50% confluence and infected with 5 μl high titer baculoviral P3

stocks per ml of culture medium. At 4 days p.i., cells were mounted on the live cell microscope described above and stained with 500 ng/ml propidium iodide (Invitrogen) or 10 μg/ml BODIPY® 558/568 C_{12} in culture medium at 26 °C for 30 min and 10 min, respectively. The marker molecules were excited with 561 nm laser light and imaged with appropriate filter settings.[44] Staining of lysosomes and mitochondria was performed with LysoTracker Deep Red and MitoTracker Deep Red, respectively (both from Life Technologies). Cells were plated and infected as described above. At 4 days p.i., cells were mounted on the live cell microscope and stained with 40 nM LysoTracker or 7 nM MitoTracker in culture medium for 15 min at 26 °C. Fluorescence was elicited with 640 nm laser light and imaged with appropriate filter settings.

For co-localization of firefly luciferase crystals with fluorescent organelle marker protein, chimeras cells were plated at 50% confluence and co-infected with identical amounts of recombinant baculovirus stocks expressing luciferase and the marker. Potential co-localization of luciferase with mCherry-KDEL (a marker for the endoplasmic reticulum (ER)) as well as Pex3-mCherry and Pex26-mCherry (peroxisome organelle markers) were analyzed 3 days and 4 days p.i., respectively. The marker proteins were excited with 561 nm laser light and imaged with appropriate filter sets.

In vivo activity of luciferase was examined by addition of the plasma membrane-permeable D-luciferin ethyl ester (Marker Gene Technologies) to cells infected with recombinant baculovirus expressing luciferase.[45] Cells were plated and infected as described above. 4 days p.i. cells were mounted on the microscope stage and imaged with DIC optics and a YFP (Yellow Fluorescent Protein) filter set for luciferin bioluminescence. During ongoing image acquisition, the culture medium was supplemented with D-luciferin ethyl ester at a final concentration of 100 μM.

C. Virus-free gene expression

The gene coding for firefly luciferase (GenBank: KC152483.1 firefly luciferase 1157–2809) was amplified from the pFastBac1 vector template (Invitrogen) by polymerase chain reaction (PCR) using primers 5′-GATCGGATCCATGGAAAACATGGAAAACGATGAAAATATTGTAGTT-3′ (sense) and 5′-GATCCTCGAGCATCTTAGCAACTGGTTTCTTAAGGATTTCTCTAAT-3′ (antisense). After restriction with NotI and BamHI, the PCR product was cloned into a modified pIEX4 expression plasmid (Novagen) lacking the internal start codon. Following transformation into competent DH5α *Escherichia coli* cells, the amplified plasmid was isolated (QIAprep Spin Miniprep Kit, Qiagen) and sequenced. Transient transfection of a monolayer culture with 0.5×10^6 Sf9 insect cells per ml was performed by lipofection with ESCORT transfection reagent (Sigma). Cells were grown and maintained in serum-free medium at 27 °C. Transfection of Sf9 cells with expression constructs encoding chimeric proteins, corresponding DNA cloning, and plasmid purification have essentially been performed as previously described.[46]

D. GFP-μNS crystal isolation and stability tests

Baculovirus-infected Sf9 cells were harvested at 96 h p.i. and lysed by incubation in hypotonic buffer (10 mM 2-[4-(2-hydroxyethyl)piperazin-1-yl]ethanesulfonic acid (HEPES) pH 7.9, 10 mM KCl, and 5 mM $MgCl_2$) for 30 min at RT. Crystals were separated from the cell debris by centrifugation for 10 min at 200× g and collected from the supernatant. Complete protease inhibitor (Roche) was added at recommended concentration to prevent crystal degradation. For dot blot stability analysis, 10 μl of a crystal suspension containing approximately 10^6 crystals per ml was pelleted for 5 min at 14 000× g and resuspended in 20 μl of an appropriate test buffer. After 1 h, 2 h, and 21 h, respectively, samples were centrifuged for 5 min at 14 000× g and 5 μl aliquots were taken from the crystal-free supernatant, followed by spotting of 1 μl of each sample on a nitrocellulose membrane. Solubilized protein from the crystals was quantified using a monoclonal anti-GFP antibody (1:1000, Roche), followed by detection with a goat anti-mouse IgG antibody coupled to horse radish peroxidase (HRP) (1:5000, Santa Cruz). In addition, stability of GFP-μNS crystals was analyzed by visual inspection using a Leica DMIRE2 fluorescence microscope with the crystals resuspended and incubated in appropriate test buffers for 30 min to 21 h.

E. Scanning electron microscopy (SEM)

After cell lysis, 50 μl GFP-μNS crystal suspension was centrifuged for 5 min at 14 000× g and the hypotonic buffer was exchanged by ultra-pure water to remove excess salt and buffer components. A 2 μl crystal aliquot was spotted onto a polished silicon sample carrier and air dried for 15 min. Scanning electron microscopy was performed using an FEI Helios Nanolap microscope operated at a chamber pressure of 10^{-6} bar with an electron acceleration voltage of 5 kV and a current of 0.89 pA.

F. Synchrotron diffraction test of GFP-μNS crystals

A suspension of isolated GFP-μNS crystals in hypotonic buffer with or without a supplement of 30% polyethylene glycol (PEG)400 (v/v) or 30% glycerol (v/v) was pipetted into a glass capillary with a diameter of 0.5 mm. After centrifugation for 15 min at 1000× g, a dense crystal pellet was clearly visible at the bottom of the capillary. The capillary was sealed with crystal wax and powder diffraction was performed with a microfocus synchrotron beam of 4 × 5 μm FWHM at the EMBL-operated P14 beamline at PETRAIII storage ring (DESY, Hamburg, Germany) with exposure times between 0.1 and 1 s, a photon flux of 10^{12} ph/s, and a photon energy of 10.00 keV.

III. RESULTS AND DISCUSSION

μNS is a protein from pathogenic ARV that causes important economic losses in poultry industry.[47] It forms ordered cytosolic inclusions inside infected cells, which are suggested to constitute together with viral RNA and structural proteins the basic scaffold for so-called viral factories that drive virus replication.[39,40] So far, the structure of μNS is unknown, most likely due to the inherent difficulty in crystallizing proteins with an intrinsic tendency to aggregate, which usually prevents obtaining soluble protein in concentrations suitable for crystallization. Since the efficient auto-assembly of μNS, particularly of the C-terminal part comprising residues 448–605, is not affected by an N-terminal GFP fusion,[39] the linked fluorescence enables direct insights into the spontaneous assembly process, which might result in a crystalline state of μNS suitable for diffraction data collection.

Luciferase catalyzes the reaction of luciferin, Mg-ATP (adeonsine triphosphate), and molecular oxygen, yielding electronically excited oxyluciferin that emits visible light during relaxation to its ground state.[48] The color of this bioluminescence, which is involved in the communication of fireflies, changes by subtle structural differences in luciferase during the emission reaction which has already been elucidated applying x-ray crystallography.[49] In cells of the firefly's lantern organ, luciferase is localized within peroxisomes due to its native C-terminal "SKL" (i.e., the tripeptide serine - lysine - leucine) import signal.[50,51] These highly dynamic organelles contain more than 50 different enzymes, some of them typically assemble into regular crystals that can be both co-crystals of a mixture of enzymes or pure crystals of one enzyme depending on the cell type involved.[8,52] Thus, peroxisomes were already known to act as a suitable cellular compartment for native protein crystallization *in vivo*. Since light excitation is not required for luciferase bioluminescence, this enzyme is commonly used in biological research as a virtually background-free luminescence reporter.[53–55] In this context, we serendipitously observed spontaneous *in vivo* crystallization of firefly luciferase in insect cells when we used this enzyme as a model to test a new method of active enzyme purification by recruitment into μNS microspheres.[40]

A. *In vivo* crystallization of firefly luciferase in Sf9 insect cells

1. Crystal growth is dynamic and not limited by cell size

Approximately 72 h after infection, the formation of needle-shaped microstructures started to be visible by DIC or phase contrast light microscopy in Sf9 insect cells infected with

recombinant baculovirus that contained the gene encoding full-length firefly luciferase. The crystal morphology was similar to that previously reported after luciferase crystallization using conventional *in vitro* techniques.[56,57] Crystal growth continued up to ∼day 5 p.i., regularly exceeding the normal dimensions of the Sf9 cells (which are ∼15–20 μm in diameter) by many times (Figure 1(a)). The majority of cells gradually lysed thereafter, largely attributable to the ongoing viral replication process rather than to plasma membrane disruption by the growth of the *in vivo* crystals. This assumption is based on visual inspection of the cell culture as well as live-cell microscopy. Degradation of the plasma membrane as a result of the tension generated by the growing crystal would lead to a sudden rupture of the membrane at one of the crystal tips, which was not observed. In contrast, we detected a slow disintegration of the plasma membrane or cell blebbing followed by plasma membrane rupture around the cell body, which is characteristic for cell lysis due to viral replication. In contrast to the previous observations with Sf9 cells that produced cathepsin B crystals,[38] no free luciferase crystals floating in the medium or attached to cell remnants were detected, indicating significantly reduced crystal stability outside the intact cell compared to cathepsin B. Remarkably, individual luciferase crystals showed a dynamic degradation and re-assembly within the same living cell over the entire growth period observed by time-lapse DIC microscopy (Figure 1(b)). This phenomenon was routinely detected for a small, but significant number of luciferase crystals in the Sf9 cell cultures. The molecular and cellular basis for this unexpected dynamic behaviour of *in vivo* crystals, which has, to our knowledge, not been reported for crystals grown in living cells so far, will be investigated in further studies. However, a direct response to changes in the environment surrounding the crystals, e.g., in the levels of recombinant gene expression or in the nutrition state of the cell, appear to be reasonable parameters to test further.

During the progress of infection, the number of crystals continuously increased until more than 50% of the cells contained up to five crystals per cell, at day 5 p.i. When several crystals were present in the same cell, they were either individually separated or stuck together to form crystalline superstructures. Luciferase crystals were characterized by extraordinary dimensions

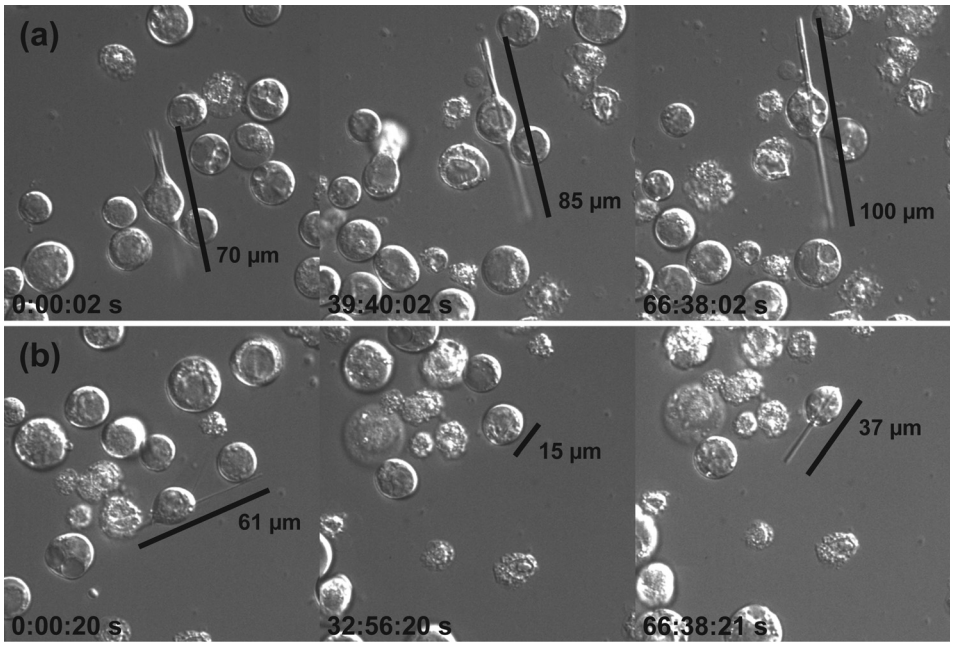

FIG. 1. Time-resolved *in vivo* crystal growth of firefly luciferase in Sf9 insect cells recorded by life-cell imaging with DIC optics. Cells were plated to 40% confluence on glass coverslips and infected with recombinant P3 luciferase virus stocks. 3 days p.i. cells were put on the live cell microscope and imaged for 67 h. (a) Luciferase crystals grew slowly over the entire period of 67 h from 70 to 100 μm in length. (b) Luciferase *in vivo* crystallization can be dynamic. In the example show, the crystal shrinks within 33 h from 61 μm to about the cell diameter (15 μm) and starts growing again to a final length of 37 μm. (Multimedia view) [URL: http://dx.doi.org/10.1063/1.4921591.1] [URL: http://dx.doi.org/10.1063/1.4921591.2]

up to 200 μm in length, depending on the respective growth state. However, the width of the crystals only varied between 1 and 3 μm (Figure 2(a)). Presenting the largest *in vivo* crystals reported so far, our study clearly demonstrates that the size of such crystals can indeed exceed the cells outer dimensions by several-fold, in strong contrast to prevalent suggestions in the current literature.[8,21] All previously reported *in vivo* crystals grown within bacteria,[14] insect cells,[16,17,58] or mammalian cells[18,20] were always restricted by the normal cell volume, without inducing alterations to cell morphology. Only our recently reported cathepsin B study provided a first indication that protein crystal length is not generally limited by the cell diameter.[38]

2. Membrane surrounded crystals originate from peroxisomes

Despite the substantial length of the luciferase *in vivo* crystals, cell viability is not affected, as revealed by the plasma membrane-impermeable DNA intercalating dye PI (Figure 2(b)). PI stains the DNA in nuclei of cells with compromised plasma membrane integrity brightly red, immediately after membrane disruption.[44] Thus, the absence of PI positive nuclear signals for cells containing large luciferase crystals provided evidence for an exceptional expansion of the plasma membrane of the living cell to cover the entire crystal, as also indicated by DIC microscopy (Figure 2(a)). Applying the lipid droplet stain BODIPY® 558/568 C_{12} with a short incubation time,[59] we detected additional internal membranes within the cell body that covered the crystals next to the plasma membrane, suggesting a growth from a specific cellular compartment (Figure 2(c)). As expected due to the presence of a corresponding native C-terminal peroxisome import signal,[50] co-infection with recombinant baculoviruses expressing genes for the

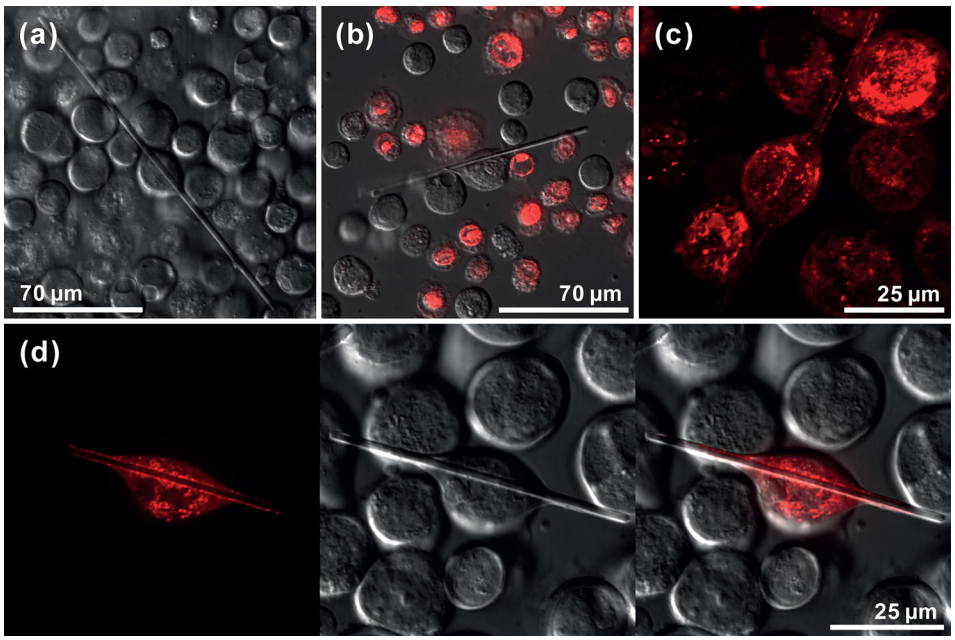

FIG. 2. Morphology and intracellular localization of *in vivo* firefly luciferase crystals. (a) Luciferase crystals can be extraordinarily long. The dimensions of the luciferase crystal inside a living cell pictured are 206 μm × 3 μm. Note that the diameter of the Sf9 cell body is only 21 μm. (b) Dead cells in the culture were identified by strong red nuclear fluorescence by addition of the membrane impermeable DNA-binding dye propidium iodide (at 500 ng/ml) to the culture medium at 4 days p.i. with recombinant baculovirus. Cells harboring crystals show no nuclear fluorescence establishing that their plasma membranes were intact. (c) Bodipy 558/568 staining a membrane surrounding a luciferase crystal. A 3D reconstruction of a z-stack of confocal fluorescence images is shown. (d) Firefly luciferase crystals are surrounded by peroxisomal membranes. Cells were co-infected with recombinant firefly luciferase and baculovirus expressing the peroxisomal membrane marker protein Pex26 fused to mCherry. Confocal images recording the DIC and the mCherry fluorescence channels were taken 4 days p.i. Note that the internal membrane surrounding the crystal is clearly labeled with the peroxisomal marker protein. (Multimedia view) [URL: http://dx.doi.org/10.1063/1.4921591.3] [URL: http://dx.doi.org/10.1063/1.4921591.4]

peroxisomal marker proteins Pex3 and Pex26[41] confirmed an origin of luciferase *in vivo* crystals from Sf9 cell peroxisomes. The fluorescence detected clearly surrounded the crystals (Figures 2(d) and S1(b)).[60] In contrast, no co-localization was detected after co-infection with an ER specific marker, mCherry-KDEL[42] (Figure S1(a)).[60] While cathepsin B that contains a native N-terminal signal sequence for rough ER import and the respective *in vivo* crystals were surrounded by membranes decorated with ribosomes, it was suggested to crystallize within the rough ER of Sf9 cells;[38] our data represent the first proof that crystallization of a recombinant protein can also occur in peroxisomes of living insect cells. Thus, depending on the protein and on the trafficking signals harboured in its primary sequence, different organelles may promote crystal formation. In mammalian Chinese hamster ovary (CHO) cells, successful human IgG crystallization was reported to occur also within the ER lumen after heterologous expression and translocation of the recombinant protein into the ER.[18,19]

Since baculovirus replication is localized within the nucleus of the infected insect cells,[61] a direct impact of viral proteins or of the replication process itself on the spontaneous crystallization of luciferase within peroxisomes appeared unlikely. However, to directly test this, we investigated virus-free transfections of Sf9 cells with a pIEX4 vector that contained the full-length luciferase cDNA. Strikingly, crystals comparable in size and morphology to those obtained in baculovirus-infected Sf9 cells grew within 2 days, i.e., even in the absence of virus (Figure S2),[60] confirming that baculovirus acts only as a gene shuttle to import the gene of interest into the insect cells. However, most crystal-positive cells contained only single crystals and also the number of cells containing crystals was reduced after direct transfection, likely attributable to decreased DNA transfection efficiency compared to the active viral DNA infection/replication process.

3. Enzyme activity or cell lysis lead to crystal degradation

Addition of a plasma membrane-permeable luciferin ethyl ester into the surrounding medium resulted in detectable bioluminescence for several minutes in living Sf9 cells (Figure S3).[60] In addition to the regular cell body, the cell protrusions induced by luciferase crystals could also be clearly traced. Mg-ATP, which is required for activation of luciferin by adenylation in the first step of the reaction,[48] was here provided by the cellular environment. Yet, the luciferase crystals completely dissolved in the intact cells within 70 s after first observable light emission, as revealed by confocal and DIC microscopy (Figure S3).[60] Degradation can be attributed to the significant conformational movements associated with the catalytic cycle which apparently destroyed the stabilizing crystal contacts.[49] The fast degradation, however, confirmed the structural and functional integrity of the luciferase protein within the *in vivo* crystal lattice. Unfortunately, this effect prevents the investigation of the structural dynamics of *in vivo* crystallized luciferase during enzymatic catalysis applying time-resolved SFX techniques. Online investigation of biomolecules in action represents one of the current challenges in XFEL science.[62,63]

Luciferase *in vivo* crystals did not exhibit significant stability after lysis of the cell membrane. When the plasma membrane is disrupted by the viral replication, crystals dissolved within hours in the surrounding culture medium (Figure 3(a)). Lysis of the cellular membranes by addition of culture medium supplemented with 0.1% (v/v) Triton X-100 lead to much faster dissolution of the crystals (Figure 3(b)). Exchange of cell medium against crystal extraction buffer (50 mM HEPES pH 7, 50 mM KCl, 2.5 mM $MgCl_2$, 2.5 mM $CaCl_2$, 2% (v/v) sucrose, and 0,1% (v/v) Triton X-100) increased the stability of the luciferase crystals up to 3 h (Figure 3(c)). This seemingly passive dissolution is in contrast to the active destruction of the crystals by activation of luciferase enzyme activity under addition of luciferin ethyl ester, where the crystals degrade within 70 s (Figure 3(d)). However, further improvement of the so far limited crystal integrity will be required to isolate sufficient amounts of intact luciferase crystals for x-ray diffraction tests and data collection at synchrotron or XFEL sources. In contrast to luciferase, cathepsin B and inosine-5′-monophosphate dehydrogenase (IMPDH) formed crystals within living Sf9 cells that were characterized by an extraordinary mechanical and chemical stability,

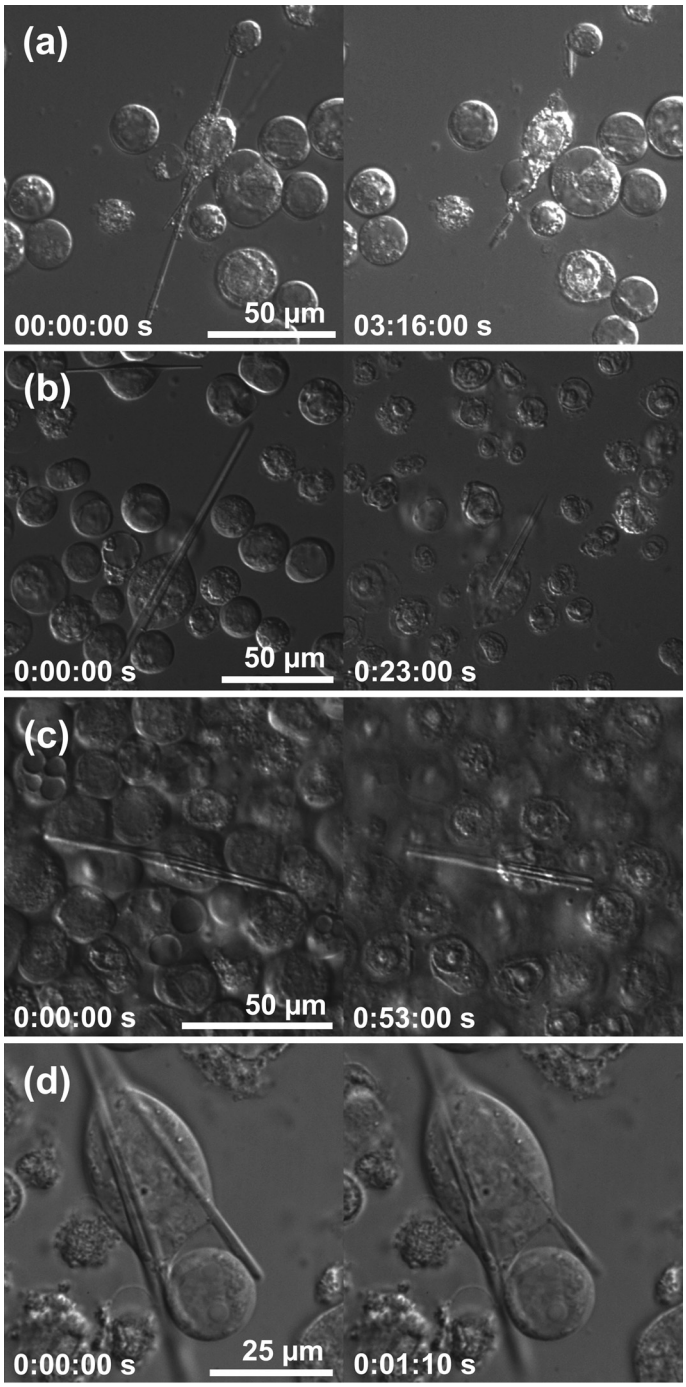

FIG. 3. Stability of firefly luciferase *in vivo* crystals. Cells were imaged 4 days p.i. with recombinant luciferase baculovirus on a live cell imaging system. (a) The cell is lysed during image acquisition by the baculovirus. Immediately after cell membrane rupture, the luciferase crystal starts to dissolve. It may take several hours for the crystal to dissolve, likely depending on how much of the, presumably protective, membranes are still left around the crystal. (b) During image acquisition, the medium was exchanged by culture medium supplemented with 0.1% Triton-X 100. In this case, cellular membranes were immediately disrupted and crystals dissolved within 30 min. (c) During image acquisition, the medium was exchanged for a crystal extraction buffer supplemented with 0.1% Triton-X 100. Cellular membranes were quickly disrupted like in (b), but the crystals dissolved much slower. Crystal length was reduced on average only by 30% during 1 h of imaging. (d) During ongoing image acquisition, medium was supplemented with 100 μM membrane-permeable D-Luciferin ethyl ester. This results in a very fast breakdown of the luciferase crystals within 70 s in the intact cells, probably caused by activation of the enzyme. (Multimedia view) [URL: http://dx.doi.org/10.1063/1.4921591.5] [URL: http://dx.doi.org/10.1063/1.4921591.6] [URL: http://dx.doi.org/10.1063/1.4921591.7] [URL: http://dx.doi.org/10.1063/1.4921591.8]

which allowed the structure elucidation of cathepsin B directly from isolated *in vivo* crystals.[30,38]

B. *In vivo* crystallization of GFP-μNS fusion protein in Sf9 insect cells

1. Nucleation and crystal growth occur in the cytosol

Production and assembly of GFP-μNS within Sf9 insect cells can be easily monitored after infection with the recombinant baculovirus due to the intrinsic GFP fluorescence In this case, GFP-μNS did not contain any native or artificially added transport signal for a specific cellular compartment. Thus, translation of the fusion protein occurred probably within the cytosol, as observed by increasing diffuse, ubiquitous fluorescence within the entire Sf9 cell starting 24 h after baculovirus infection. Accumulation of GFP molecules into several tiny dots at 77 h p.i. indicated formation of initial crystal nuclei (Figure 4). However, most crystal nuclei exhibited a transient character. Only few crystal nuclei grew into macroscopic visible structures that reached final dimensions of 10 μm in length and 3 μm in width at day 4 p.i., but without exceeding the regular cell diameter. Consequently, the morphology of the Sf9 cells was not

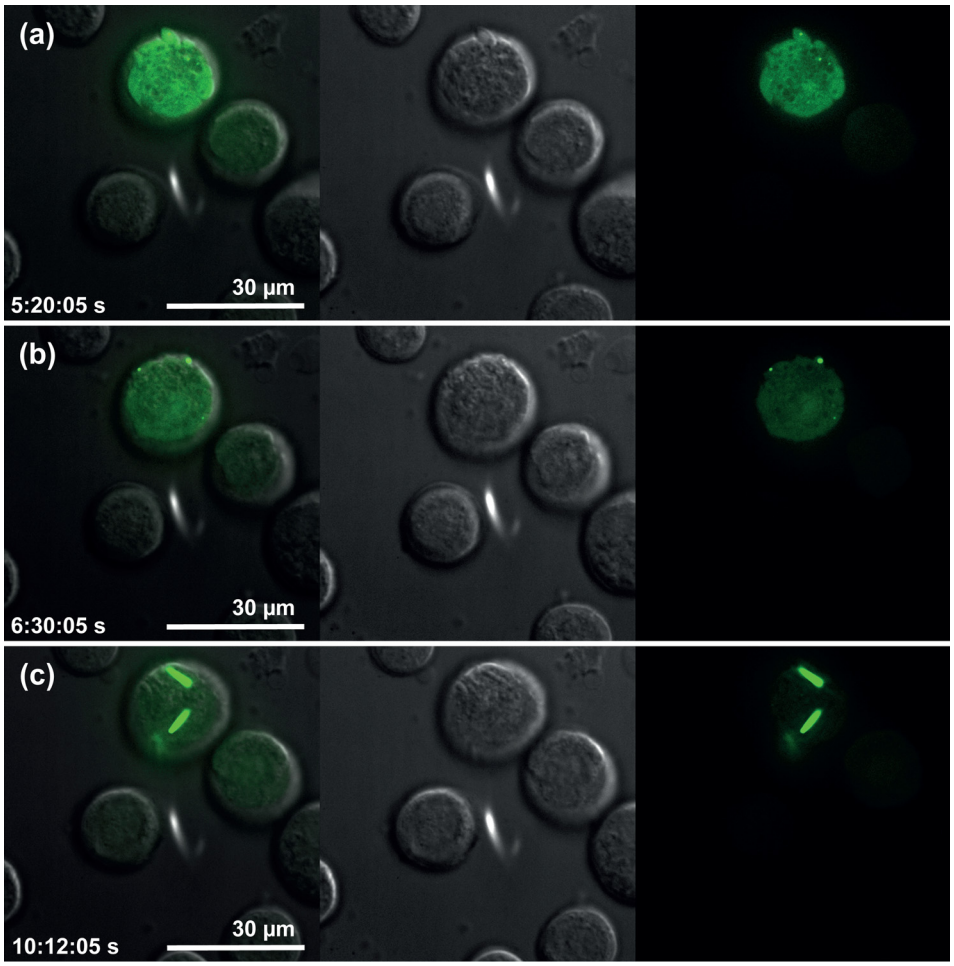

FIG. 4. Time-resolved *in vivo* crystal growth of GFP-μNS in Sf9 insect cells recorded by life-cell imaging with DIC optics and GFP fluorescence. Crystal growth was imaged 3 days p.i. over night. (a) GFP-μNS is expressed in the cytoplasm and displays a ubiquitous diffuse fluorescence together with a variable number of dots with higher fluorophore concentration. (b) Some of those dots apparently act as crystallization points and start to grow by accumulating more protein. (c) Crystals are fully grown. Background fluorescence in the cytoplasm is still visible as well as several crystallization nuclei that did not grow out into a full crystal. (Multimedia view) [URL: http://dx.doi.org/10.1063/1.4921591.9]

affected by GFP-μNS *in vivo* crystallization, despite being much more efficient than the crystallization of luciferase. Almost all cells in the entire culture were found to be positive for GFP-μNS crystals. Remarkably, neither dynamic crystal growth nor crystal degradation, as observed for luciferase, was detected for these macroscopic GFP-μNS structures.

The mature GFP-μNS assemblies exhibited an elongated, almost needle-shaped morphology with a hexagonal cross section (Figure 5(b)), but, in contrast to luciferase, bundled needles forming star-shaped superstructures were observed (Figures 5(a) and 5(c)). Crystals were visible in living cells showing no PI staining as well as in cells positively stained with PI (Figure 5(d)). This result shows that general cell viability was not affected by GFP-μNS crystallization and that these crystals exhibit a much higher intrinsic stability compared to luciferase crystals.

A strong intrinsic tendency for auto-assembly represents the physiological function of the viral μNS domains in the process of viral replication factory formation, natively occurring in the cytosol of reovirus-infected cells.[39,40] As reported above for luciferase, *in vivo* crystallization of GFP-μNS did not depend on baculovirus infection. Spontaneous assembly formation was previously detected in primary cultures of chicken embryo fibroblasts (CEF) directly transfected with a plasmid expressing GFP-μNS.[39] The mature GFP-μNS assemblies grown in CEF were comparable in size and morphology to the structures observed after baculovirus infection of insect cells.

Another remarkable phenomenon that has not been described before is that different proteins can crystallize in the same cell (Figure S4).[60] After co-infection with Bac-luc and Bac-GFP-μNS viral stocks, following the previously described protocol for co-infection experiments with recombinant viruses expressing marker proteins, both *in vivo* crystal species were simultaneously detected in some cells. These crystals showed no obvious alterations in their

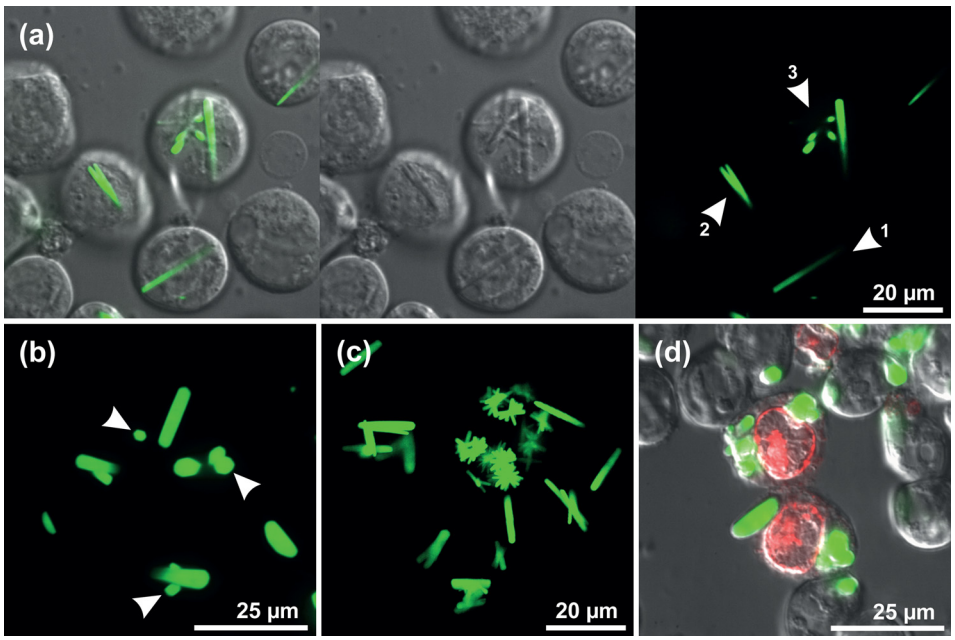

FIG. 5. Morphology of GFP-μNS *in vivo* crystals. Cells were infected with recombinant GFP-μNS baculovirus and incubated for 3 days. Subsequently, cells were imaged on a confocal fluorescence microscope system. (a) Mostly, rod-like crystals can be seen, routinely with several crystals per cell. Crystals inside cells can be separated (arrow 1) or lying parallel to each other (arrow 2), or they arranged in a star-like fashion (arrow 3). The length of the crystals does not exceed the diameter of the cell body. The diameter of the crystals varies between <1 and 5 μm. (b) The fluorescent GFP-μNS crystals show a hexagonal profile in confocal cross sections (arrows). (c) A 3D reconstruction of a z-stack of confocal fluorescence images is shown. Several packs of crystals in a star like arrangement can be seen. (d) Dead cells were identified by adding the membrane impermeable dye propidium iodide (500 ng/ml) at 4 days p.i. Note that crystals are visible in both cells with or without red nuclear fluorescence, demonstrating that GFP-μNS crystals are stable after cell lysis caused by baculovirus reproduction. (Multimedia view) [URL: http://dx.doi.org/10.1063/1.4921591.10]

morphology compared to corresponding crystals individually grown in different cells, indicating no direct impact of GFP-μNS and luciferase on each other during crystal formation. This can be explained by crystallization events occurring in different cellular compartments. As shown in this study, luciferase crystals grow in peroxisomes, while GFP-μNS is suggested to crystallize within the cytosol. Thus, expression of either of the proteins did not change the cellular environment of the other.

2. Isolated crystals show intrinsic stability

As previously reported for cathepsin B,[30,38] isolation of *in vivo* grown GFP-μNS crystals was performed by membrane disruption and differential centrifugation without apparent crystal damage. Since cell lysis is associated with extreme changes in the environmental conditions of the *in vivo* crystals, the identification of buffers conferring optimal stability represents an important requirement to maintain maximum crystalline order after extraction. We applied dot blot techniques to enable large-scale screening of various environmental conditions, including pH value and different concentrations of cryo-protectants. Extracted GFP-μNS crystals were incubated for up to 21 h in the test buffer, followed by centrifugation and highly sensitive immunochemical detection of solubilized protein in the supernatants (Figure S5(a)).[60] The isolated crystals were stable in high- or low-salt solutions and acidic buffers but became soluble in alkaline buffers above pH 10. Moreover, glycerol and PEG 400, both up to 40%, were identified as suitable cryo-protectants for potential single-crystal diffraction tests applying synchrotron radiation. Supplement of PEG400 increased the stability of GFP-μNS crystals, in general, even preventing the rapid dissolution at pH 10. Our screening experiments additionally revealed that Mg^{2+} ions were essential for the stability of the macroscopic structure of GFP-μNS crystals outside of their natural cellular environment. Disruption of the cell membrane in buffers without Mg^{2+} ions resulted in immediate diversification of the crystals (Figure S5(b)).[60] Most noteworthy, GFP-μNS *in vivo* crystals withstood even dry conditions in vacuum during SEM analysis without any disruption into small fragments, as usually expected for protein crystals, revealing the high intrinsic stability (Figure 6(a)). Although SEM analysis showed roundish edges of the individual assemblies, the perfectly flat surfaces strongly supported a crystalline character of the GFP-μNS assemblies.

3. Powder diffraction reveals crystalline state

The formation of GFP-μNS assemblies within living cells has previously been reported, but the detected microstructures were not considered to consist of an ordered crystalline lattice so

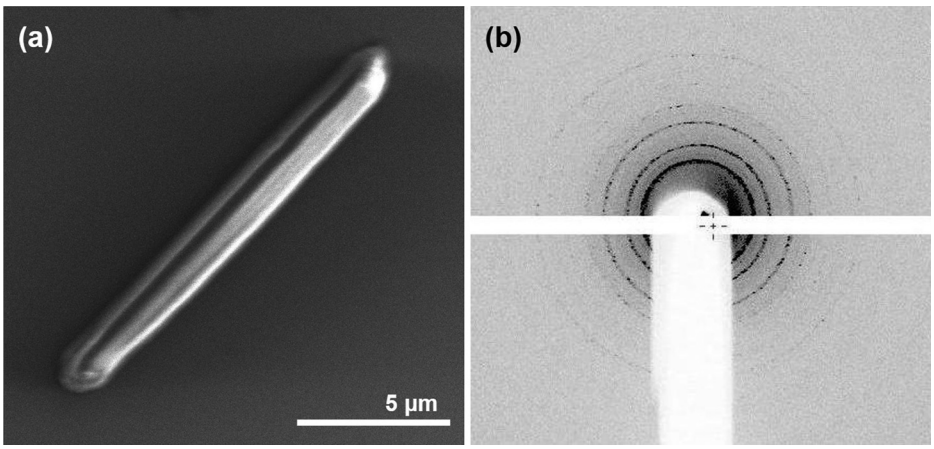

FIG. 6. Surface morphology and diffraction quality of GFP-μNS crystals. (a) Extracted GFP-μNS crystals were spotted onto a sample carrier and applied to SEM. The depicted crystal has a smooth and highly regular surface and a size of 15 μm $\times$ 2 μm. Moreover, it retains its rod-shaped morphology even under vacuum conditions, indicating its remarkable intrinsic stability. (b) GFP-μNS crystals were pelleted in a glass capillary and analyzed by synchrotron powder diffraction experiments. The pattern reveals weak diffraction of approximately 30 Å, confirming a crystalline state.

far.[39,40] However, the exceptional stability and the regular crystalline appearance of the GFP-μNS *in vivo* crystals (Figures 5(b) and 6(a)) determined in this study qualified them for synchrotron diffraction tests. Crystals grown in suspension culture of baculovirus-infected Sf9 cells were extracted 4 days p.i. and centrifuged to remove excess of cell remnants. Powder diffraction tests have been performed at the EMBL-operated microfocus beamline P14 of the PETRA III synchrotron source (DESY, Hamburg, Germany). The detection of typical Debeye-Scherrer rings generally verified the crystallinity of the GFP-μNS assemblies (Figure 6(b)). Amorphous material would have produced a broad and continuous background signal instead of sharp diffraction rings, which are the result of constructive interference of the incident x-rays with the electrons in the well-ordered lattice satisfying Bragg's law. However, the very low maximum resolution of around 30 Å detected for the diffracted x-rays that have not been improved so far by testing other buffer conditions, e.g., including 30% PEG 400 or 30% glycerol as cryoprotectants for potential single-crystal diffraction experiments, prevented the use of GFP-μNS *in vivo* crystals as suitable targets for x-ray crystallography. Assuming that μNS forms the regular crystal lattice driven by its high intrinsic assembly tendency,[39] the fusion of GFP may have disturbed crystal order by increasing the overall flexibility of the protein, thus interfering with a well-ordered crystal lattice. On the other hand, a direct impact of the extraction process and the non-native buffer conditions which might damage the *in vivo* crystals can also not be excluded. Consequently, *in cellulo* diffraction data collection represents a suitable trail to compare the diffraction data quality before and after crystal isolation. Interestingly, substitution of the GFP moiety by the C-terminal tail of μNS significantly changed the morphology of the μNS crystals into a globular shape.[39] The crystalline character and the diffraction properties of globular pure μNS assemblies are currently under investigation.

IV. CONCLUSIONS

Convincing examples, particularly the pioneering structure elucidation of insect virus polyhedra[16,21,36] and of the native *B. thuringiensis* toxin Cry3A,[34] but also the high-resolution structure determination of cathepsin B,[30,35] as well as the SFX diffraction tests performed with protein crystals formed in mammalian and cockroach cells,[20] already demonstrated the feasibility to implement *in vivo* crystallography at XFEL and third-generation synchrotron sources as a new strategy for structural biology. However, the general applicability to crystallize any kind of protein within a living cell is so far questionable, even if the number of spontaneous crystallization observations significantly increased, involving various cell types.

In the present study, we report the crystal formation of two new examples, firefly luciferase and avian reovirus μNS, upon high-level heterologous expression in living Sf9 insect cells. Together with polyhedrin from *Bombyx mori* cytoplasmic polyhedrosis virus,[64] cathepsin B and IMPDH from *T. brucei*[38] as well as calcineurin,[17] six successful *in vivo* crystallization events are now described. All of those examples occur during gene over-expression in these cells, indicating a more general phenomenon. Providing first evidence that recombinant proteins can crystallize in peroxisomes of insect cells, we identified the cellular compartment of crystal origin as an initial parameter that could influence successful crystal growth. Most strikingly, our live-cell imaging studies not only provided real-time insights into the spontaneous crystallization process in living cells but also clearly revealed that the normal outer cell dimensions do not limit the crystal size and that the *in vivo* crystallization process can be highly dynamic, disproving the previous suggestions. These important results represent the starting point for a detailed and systematic investigation of the cellular crystallization mechanisms in living insect cells, which is currently ongoing in our group. The identification of additional cellular parameters next to the compartment will enable a systematic screening of target proteins to optimize the success rate of this novel approach. The dynamics detected for luciferase *in vivo* crystals suggest an active involvement of cellular processes, e.g., protein and membrane transport mechanisms, in intracellular crystallization, which will be investigated and identified in future studies.

The confirmation that *in vivo* crystals grown within insect cells are not necessarily characterized by an extraordinary intrinsic stability outside of their natural environment, as we have previously suggested based on our experience with cathepsin B and IMPDH[38] and shown here for GFP-μNS, represents another important result of our study. This shifts diffraction data collection from *in vivo* crystals directly within the living cells, denoted as the "*in cellulo*" approach,[21] into focus, which would avoid crystal damage arising from the non-physiological environmental conditions after crystal extraction. *In cellulo* data collection has already been tested by injecting tiny bacterial cells into XFEL pulses[34] as well as by mounting frozen intact insect cells directly in a synchrotron beam,[21] both providing first evidence that background scattering from other cell components did not obscure the Bragg diffraction from *in vivo* grown protein crystals. Due to their enormous size, the luciferase crystals reported here represent highly interesting candidates for an *in cellulo* data collection experiment using synchrotron radiation in the future. However, particularly, the microjet-based sample injection techniques of the SFX approach need optimization, since the comparatively large insect cells require large gas focused liquid jets to avoid clogging of the nozzle, which in turn would result in high background scattering.[20] On the other hand, the systematic investigation of crystal stabilization trials directly in the living cell or the improvement of the crystal extraction procedure for instable crystals will enhance the chance to collect suitable diffraction data from *in vivo* crystals applying well-established SFX or serial synchrotron crystallography techniques.[30,35,65] In this context, the dot blot approach proposed in this study appears to be highly suitable for large-scale screening of appropriate buffer conditions in terms of securing maximum stability of isolated *in vivo* crystals.

Comparing the crystal morphology of luciferase and GFP-μNS with that of previously reported *T. brucei* cathepsin B[30] and IMPDH[38] indicates a preference for needle-like crystals *in vivo*, which renders conventional synchrotron diffraction data collection difficult due to the small size of the short crystal axis. Moreover, flow alignment of the elongated cathepsin B *in vivo* crystals during microjet-based sample injection increased the required amount of diffraction data to cover all crystal orientations in SFX experiments.[30] On the other hand, a preferred orientation due to the needle-like shape could help to obtain angular information in SFX experiments, particularly if fixed-target sample delivery that was recently reported for SFX techniques[66] will be improved to allow sample mounting for in a specific, well-defined orientation in the future. Full sampling of reciprocal space will be allowed by the use of a goniometer stage that rotates the normal vector of the fixed target support relative to the incident XFEL pulses, while proof-of-principle experiments indicated dramatically reduced sample consumption compared to flowing jet methods.[66]

Successful protein crystallization within living cells would abolish the need for time-consuming optimization of recombinant protein production and conventional crystallization strategies. Thus, this approach offers exciting new possibilities for proteins that do not form crystals suitable for x-ray diffraction *in vitro*, if the associated cellular mechanisms will be understood in more detail in the future.

ACKNOWLEDGMENTS

The x-ray diffraction experiment was carried out at beamline P14 of the PETRA III synchrotron source operated by the European Molecular Biology Laboratory (EMBL) at the German Electron Synchrotron (DESY) in Hamburg, Germany. Support from Dr. Gleb Bourenkov was strongly acknowledged. R.S. thanks the Graduate School for Computing in Medicine and Life Sciences at the University of Lübeck for funding. L.R., M.K., D.R., and C.B. thank the German Federal Ministry for Education and Research (BMBF) for funding (Grant Nos. 01KX0806 and 01KX0807). L.R., M.D., and C.B. acknowledge support from the BMBF in the context of the Röntgen-Angström-Cluster (Grant No. 05K12GU3). J.M.-C. and A.B.-N. acknowledge support from the Spanish Ministerio Economía y Competitividad (MINECO, Grant No. BFU2013-43513-R). I.V.M., R.D., and L.R. are grateful for support from the DFG Cluster of Excellence "Inflammation at Interfaces" (EXC 306).

[1]R. J. Southworth-Davies, M. A. Medina, I. Carmichael, and E. F. Garman, "Observation of decreased radiation damage at higher dose rates in room temperature protein crystallography," Structure **15**, 1531–1541 (2007).
[2]J. M. Holton and K. A. Frankel, "The minimum crystal size needed for a complete diffraction data set," Acta Crystallogr., Sect. D: Biol. Crystallogr. **66**, 393–408 (2010).
[3]R. Henderson, "Cryoprotection of protein crystals against radiation damage in electron and X-ray diffraction," Proc. R. Soc. London, Ser. B **241**, 6–8 (1990).
[4]E. F. Garman and T. R. Schneider, "Macromolecular Cryocrystallography," J. Appl. Crystallogr. **30**, 211–237 (1997).
[5]R. M. Bill, P. J. Henderson, S. Iwata, E. R. Kunji, H. Michel, R. Neutze, S. Newstead, B. Poolman, C. G. Tate, and H. Vogel, "Overcoming barriers to membrane protein structure determination," Nat. Biotechnol. **29**, 335–340 (2011).
[6]A. McPherson and J. A. Gavira, "Introduction to protein crystallization," Acta Crystallogr., Sect. F: Struct. Biol. Commun. **70**, 2–20 (2014).
[7]M. Weselak, M. G. Patch, T. L. Selby, G. Knebel, and R. C. Stevens, "Robotics for automated crystal formation and analysis," Methods Enzymol. **368**, 45–76 (2003).
[8]J. P. K. Doye and W. C. K. Poon, "Protein crystallization *in vivo*," Curr. Opin. Colloid Interface Sci. **11**, 40–46 (2006).
[9]A. McPherson, *Crystallization of Biological Macromolecules* (Cold Spring Harbor Laboratory Press, 1999).
[10]P. M. Colman, E. Suzuki, and A. Van Donkelaar, "The structure of cucurbitin: Subunit symmetry and organization *in situ*," Eur. J. Biochem. **103**, 585–588 (1980).
[11]K. Müntz, "Deposition of storage proteins," Plant Mol. Biol. **38**, 77–99 (1998).
[12]G. Dodson and D. Steiner, "The role of assembly in insulin's biosynthesis," Curr. Opin. Struct. Biol. **8**, 189–194 (1998).
[13]M. Veenhuis, J. A. Kiel, and I. J. van der Klei, "Peroxisome assembly in yeast," Microsc. Res. Tech. **61**, 139–150 (2003).
[14]H. Höfte and H. R. Whiteley, "Insecticidal crystal proteins of *Bacillus thuringiensis*," Microbiol. Rev. **53**, 242–255 (1989).
[15]G. F. Rohrmann, "Polyhedrin structure," J. Gen. Virol. **67**, 1499–1513 (1986).
[16]F. Coulibaly, E. Chiu, K. Ikeda, S. Gutmann, P. W. Haebel, C. Schulze-Briese, H. Mori, and P. Metcalf, "The molecular organization of cypovirus polyhedra," Nature **446**, 97–101 (2007).
[17]G. Y. Fan, F. Maldonado, Y. Zhang, R. Kincaid, M. H. Ellisman, and L. N. Gastinel, "*In vivo* calcineurin crystals formed using the baculovirus expression system," Microsc. Res. Tech. **34**, 77–86 (1996).
[18]H. Hasegawa, J. Wendling, F. He, E. Trilisky, R. Stevenson, H. Franey, F. Kinderman, G. Li, D. M. Piedmonte, T. Osslund, M. Shen, and R. R. Ketchem, "*In vivo* crystallization of human IgG in the endoplasmic reticulum of engineered Chinese hamster ovary (CHO) cells," J. Biol. Chem. **286**, 19917–19931 (2011).
[19]H. Hasegawa, C. Forte, I. Barber, S. Turnbaugh, J. Stoops, M. Shen, and A. C. Lim, "Modulation of *in vivo* IgG crystallization in the secretory pathway by heavy chain isotype class switching and N-linked glycosylation," Biochim. Biophys. Acta **1843**, 1325–1338 (2014).
[20]F. X. Gallat, N. Matsugaki, N. P. Coussens, K. J. Yagi, M. Boudes, T. Higashi, D. Tsuji, Y. Tatano, M. Suzuki, E. Mizohata, K. Tono, Y. Joti, T. Kameshima, J. Park, C. Song, T. Hatsui, M. Yabashi, E. Nango, K. Itoh, F. Coulibaly, S. Tobe, S. Ramaswamy, B. Stay, S. Iwata, and L. M. Chavas, "*In vivo* crystallography at X-ray free-electron lasers: the next generation of structural biology?," Philos. Trans. R. Soc. London, Ser. B: Biol. Sci. **369**, 20130497 (2014).
[21]D. Axford, X. Ji, D. I. Stuart, and G. Sutton, "In cellulo structure determination of a novel cypovirus polyhedrin," Acta Crystallogr., Sect. D: Biol. Crystallogr. **70**, 1435–1441 (2014).
[22]R. Neutze, R. Wouts, D. van der Spoel, E. Weckert, and J. Hajdu, "Potential for biomolecular imaging with femtosecond X-ray pulses," Nature **406**, 752–757 (2000).
[23]H. N. Chapman, P. Fromme, A. Barty, T. A. White, R. A. Kirian, A. Aquila, M. S. Hunter, J. Schulz, D. P. DePonte, U. Weierstall, R. B. Doak, F. R. Maia, A. V. Martin, I. Schlichting, L. Lomb, N. Coppola, R. L. Shoeman, S. W. Epp, R. Hartmann, D. Rolles, A. Rudenko, L. Foucar, N. Kimmel, G. Weidenspointner, P. Holl, M. Liang, M. Barthelmess, C. Caleman, S. Boutet, M. J. Bogan, J. Krzywinski, C. Bostedt, S. Bajt, L. Gumprecht, B. Rudek, B. Erk, C. Schmidt, A. Hömke, C. Reich, D. Pietschner, L. Strüder, G. Hauser, H. Gorke, J. Ullrich, S. Herrmann, G. Schaller, F. Schopper, H. Soltau, K. U. Kühnel, M. Messerschmidt, J. D. Bozek, S. P. Hau-Riege, M. Frank, C. Y. Hampton, R. G. Sierra, D. Starodub, G. J. Williams, J. Hajdu, N. Timneanu, M. M. Seibert, J. Andreasson, A. Rocker, O. Jönsson, M. Svenda, S. Stern, K. Nass, R. Andritschke, C. D. Schröter, F. Krasniqi, M. Bott, K. E. Schmidt, X. Wang, I. Grotjohann, J. M. Holton, T. R. Barends, R. Neutze, S. Marchesini, R. Fromme, S. Schorb, D. Rupp, M. Adolph, T. Gorkhover, I. Andersson, H. Hirsemann, G. Potdevin, H. Graafsma, B. Nilsson, and J. C. Spence, "Femtosecond X-ray protein nanocrystallography," Nature **470**, 73–77 (2011).
[24]S. Boutet, L. Lomb, G. J. Williams, T. R. Barends, A. Aquila, R. B. Doak, U. Weierstall, D. P. DePonte, J. Steinbrener, R. L. Shoeman, M. Messerschmidt, A. Barty, T. A. White, S. Kassemeyer, R. A. Kirian, M. M. Seibert, P. A. Montanez, C. Kenney, R. Herbst, P. Hart, J. Pines, G. Haller, S. M. Gruner, H. T. Philipp, M. W. Tate, M. Hromalik, L. J. Koerner, N. van Bakel, J. Morse, W. Ghonsalves, D. Arnlund, M. J. Bogan, C. Caleman, R. Fromme, C. Y. Hampton, M. S. Hunter, L. C. Johansson, G. Katona, C. Kupitz, M. Liang, A. V. Martin, K. Nass, L. Redecke, F. Stellato, N. Timneanu, D. Wang, N. A. Zatsepin, D. Schafer, J. Defever, R. Neutze, P. Fromme, J. C. Spence, H. N. Chapman, and I. Schlichting, "High-resolution protein structure determination by serial femtosecond crystallography," Science **337**, 362–364 (2012).
[25]T. A. White, R. A. Kirian, A. V. Martin, A. Aquila, K. Nass, A. Barty, and H. N. Chapman, "CrystFEL: A software suite for snapshot serial crystallography," J. Appl. Crystallogr. **45**, 335–341 (2012).
[26]A. Barty, R. A. Kirian, F. R. N. C. Maia, M. Hantke, C. H. Yoon, T. A. White, and H. N. Chapman, "Cheetah: Software for high-throughput reduction and analysis of serial femtosecond X-ray diffraction data," J. Appl. Crystallogr. **47**, 1118–1131 (2014).
[27]R. A. Kirian, T. A. White, J. M. Holton, H. N. Chapman, P. Fromme, A. Barty, L. Lomb, A. Aquila, F. R. Maia, A. V. Martin, R. Fromme, X. Wang, M. S. Hunter, K. E. Schmidt, and J. C. Spence, "Structure-factor analysis of femtosecond microdiffraction patterns from protein nanocrystals," Acta Crystallogr., Sect. A: Found. Crystallogr. **67**, 131–140 (2011).
[28]D. P. DePonte, U. Weierstall, K. Schmidt, J. Warner, D. Starodub, J. C. H. Spence, and R. B. Doak, "Gas dynamic virtual nozzle for generation of microscopic droplet streams," J. Phys. D: Appl. Phys. **41**, 195505 (2008).

[29]U. Weierstall, D. James, C. Wang, T. A. White, D. Wang, W. Liu, J. C. Spence, R. Bruce Doak, G. Nelson, P. Fromme, R. Fromme, I. Grotjohann, C. Kupitz, N. A. Zatsepin, H. Liu, S. Basu, D. Wacker, G. W. Han, V. Katritch, S. Boutet, M. Messerschmidt, G. J. Williams, J. E. Koglin, M. Seibert, M. Klinker, C. Gati, R. L. Shoeman, A. Barty, H. N. Chapman, R. A. Kirian, K. R. Beyerlein, R. C. Stevens, D. Li, S. T. Shah, N. Howe, M. Caffrey, and V. Cherezov, "Lipidic cubic phase injector facilitates membrane protein serial femtosecond crystallography," Nat. Commun. **5**, 3309 (2014).
[30]L. Redecke, K. Nass, D. P. DePonte, T. A. White, D. Rehders, A. Barty, F. Stellato, M. Liang, T. R. Barends, S. Boutet, G. J. Williams, M. Messerschmidt, M. M. Seibert, A. Aquila, D. Arnlund, S. Bajt, T. Barth, M. J. Bogan, C. Caleman, T. C. Chao, R. B. Doak, H. Fleckenstein, M. Frank, R. Fromme, L. Galli, I. Grotjohann, M. S. Hunter, L. C. Johansson, S. Kassemeyer, G. Katona, R. A. Kirian, R. Koopmann, C. Kupitz, L. Lomb, A. V. Martin, S. Mogk, R. Neutze, R. L. Shoeman, J. Steinbrener, N. Timneanu, D. Wang, U. Weierstall, N. A. Zatsepin, J. C. Spence, P. Fromme, I. Schlichting, M. Duszenko, C. Betzel, and H. N. Chapman, "Natively inhibited *Trypanosoma brucei* cathepsin B structure determined by using an X-ray laser," Science **339**, 227–230 (2013).
[31]J. Kern, R. Alonso-Mori, R. Tran, J. Hattne, R. J. Gildea, N. Echols, C. Glöckner, J. Hellmich, H. Laksmono, R. G. Sierra, B. Lassalle-Kaiser, S. Koroidov, A. Lampe, G. Han, S. Gul, D. Difiore, D. Milathianaki, A. R. Fry, A. Miahnahri, D. W. Schafer, M. Messerschmidt, M. M. Seibert, J. E. Koglin, D. Sokaras, T. C. Weng, J. Sellberg, M. J. Latimer, R. W. Grosse-Kunstleve, P. H. Zwart, W. E. White, P. Glatzel, P. D. Adams, M. J. Bogan, G. J. Williams, S. Boutet, J. Messinger, A. Zouni, N. K. Sauter, V. K. Yachandra, U. Bergmann, and J. Yano, "Simultaneous femtosecond X-ray spectroscopy and diffraction of photosystem II at room temperature," Science **340**, 491–495 (2013).
[32]T. R. Barends, L. Foucar, R. L. Shoeman, S. Bari, S. W. Epp, R. Hartmann, G. Hauser, M. Huth, C. Kieser, L. Lomb, K. Motomura, K. Nagaya, C. Schmidt, R. Strecker, D. Anielski, R. Boll, B. Erk, H. Fukuzawa, E. Hartmann, T. Hatsui, P. Holl, Y. Inubushi, T. Ishikawa, S. Kassemeyer, C. Kaiser, F. Koeck, N. Kunishima, M. Kurka, D. Rolles, B. Rudek, A. Rudenko, T. Sato, C. D. Schroeter, H. Soltau, L. Strueder, T. Tanaka, T. Togashi, K. Tono, J. Ullrich, S. Yase, S. I. Wada, M. Yao, M. Yabashi, K. Ueda, and I. Schlichting, "Anomalous signal from S atoms in protein crystallographic data from an X-ray free-electron laser," Acta Crystallogr., Sect. D: Biol. Crystallogr. **69**, 838–842 (2013).
[33]T. R. Barends, L. Foucar, S. Botha, R. B. Doak, R. L. Shoeman, K. Nass, J. E. Koglin, G. J. Williams, S. Boutet, M. Messerschmidt, and I. Schlichting, "De novo protein crystal structure determination from X-ray free-electron laser data," Nature **505**, 244–247 (2014).
[34]M. R. Sawaya, D. Cascio, M. Gingery, J. Rodriguez, L. Goldschmidt, J. P. Colletier, M. M. Messerschmidt, S. Boutet, J. E. Koglin, G. J. Williams, A. S. Brewster, K. Nass, J. Hattne, S. Botha, R. B. Doak, R. L. Shoeman, D. P. DePonte, H. W. Park, B. A. Federici, N. K. Sauter, I. Schlichting, and D. S. Eisenberg, "Protein crystal structure obtained at 2.9 Å resolution from injecting bacterial cells into an X-ray free-electron laser beam," Proc. Natl. Acad. Sci. U.S.A. **111**, 12769–12774 (2014).
[35]C. Gati, G. Bourenkov, M. Klinge, D. Rehders, F. Stellato, D. Oberthür, O. Yefanov, B. P. Sommer, S. Mogk, M. Duszenko, C. Betzel, T. R. Schneider, H. N. Chapman, and L. Redecke, "Serial crystallography on *in vivo* grown microcrystals using synchrotron radiation," IUCrJ **1**, 87–94 (2014).
[36]F. Coulibaly, E. Chiu, S. Gutmann, C. Rajendran, P. W. Haebel, K. Ikeda, H. Mori, V. K. Ward, C. Schulze-Briese, and P. Metcalf, "The atomic structure of baculovirus polyhedra reveals the independent emergence of infectious crystals in DNA and RNA viruses," Proc. Natl. Acad. Sci. U.S.A. **106**, 22205–22210 (2009).
[37]X. Ji, G. Sutton, G. Evans, D. Axford, R. Owen, and D. I. Stuart, "How baculovirus polyhedra fit square pegs into round holes to robustly package viruses," EMBO J. **29**, 505–514 (2010).
[38]R. Koopmann, K. Cupelli, L. Redecke, K. Nass, D. P. Deponte, T. A. White, F. Stellato, D. Rehders, M. Liang, J. Andreasson, A. Aquila, S. Bajt, M. Barthelmess, A. Barty, M. J. Bogan, C. Bostedt, S. Boutet, J. D. Bozek, C. Caleman, N. Coppola, J. Davidsson, R. B. Doak, T. Ekeberg, S. W. Epp, B. Erk, H. Fleckenstein, L. Foucar, H. Graafsma, L. Gumprecht, J. Hajdu, C. Y. Hampton, A. Hartmann, R. Hartmann, G. Hauser, H. Hirsemann, P. Holl, M. S. Hunter, S. Kassemeyer, R. A. Kirian, L. Lomb, F. R. Maia, N. Kimmel, A. V. Martin, M. Messerschmidt, C. Reich, D. Rolles, B. Rudek, A. Rudenko, I. Schlichting, J. Schulz, M. M. Seibert, R. L. Shoeman, R. G. Sierra, H. Soltau, S. Stern, L. Strüder, N. Timneanu, J. Ullrich, X. Wang, G. Weidenspointner, U. Weierstall, G. J. Williams, C. B. Wunderer, P. Fromme, J. C. Spence, T. Stehle, H. N. Chapman, C. Betzel, and M. Duszenko, "*In vivo* protein crystallization opens new routes in structural biology," Nat. Methods **9**, 259–262 (2012).
[39]A. Brandariz-Nuñez, R. Menaya-Vargas, J. Benavente, and J. A. Martínez-Costas, "Versatile molecular tagging method for targeting proteins to avian reovirus muNS inclusions. Use in protein immobilization and purification," PLoS One **5**, e13961 (2010).
[40]A. Brandariz-Nuñez, R. Menaya-Vargas, J. Benavente, and J. Martínez-Costas, "Avian reovirus NS protein forms homo-oligomeric inclusions in a microtubule-independent fashion, which involves specific regions of its C-terminal domain," J. Virol. **84**, 4289–4301 (2010).
[41]S. Ally, A. G. Larson, K. Barlan, S. E. Rice, and V. I. Gelfand, "Opposite-polarity motors activate one another to trigger cargo transport in live cells," J. Cell Biol. **187**, 1071–1082 (2009).
[42]N. Zurek, L. Sparks, and G. Voeltz, "Reticulon short hairpin transmembrane domains are used to shape ER tubules," Traffic **12**, 28–41 (2011).
[43]J. A. Steinkamp, R. C. Habbersett, and C. C. Stewart, "A modular detector for flow cytometric multicolor fluorescence measurements," Cytometry **8**, 353–365 (1987).
[44]I. Majoul, L. Gao, E. Betzig, D. Onichtchouk, E. Butkevich, Y. Kozlov, F. Bukauskas, M. L. V. Bennett, J. Lippincott-Schwartz, and R. Duden, "Fast structural responses of gap junction membrane domains to AB5 toxins," Proc. Natl. Acad. Sci. U.S.A. **110**, E4125–4133 (2013).
[45]F. F. Craig, A. C. Simmonds, D. Watmore, F. McCapra, and M. R. White, "Membrane-permeable luciferin esters for assay of firefly luciferase in live intact cells," Biochem. J. **276**, 637–641 (1991).
[46]I. Majoul, M. Straub, S. W. Hell, R. Duden, and H. D. Söling, "KDEL-cargo regulates interactions between proteins involved in COPI vesicle traffic: Measurements in living cells using FRET," Dev. Cell **1**, 139–153 (2001).
[47]R. C. Jones, "Avian reovirus infections," Rev. Sci. Tech. **19**, 614–625 (2000).
[48]L. Pinto da Silva and J. C. Esteves da Silva, "Firefly chemiluminescence and bioluminescence: Efficient generation of excited states," ChemPhysChem **13**, 2257–2262 (2012).

[49]T. Nakatsu, S. Ichiyama, J. Hiratake, A. Saldanha, N. Kobashi, K. Sakata, and H. Kato, "Structural basis for the spectral difference in luciferase bioluminescence," Nature **440**, 372–376 (2006).
[50]G. A. Keller, S. Gould, M. Deluca, and S. Subramani, "Firefly luciferase is targeted to peroxisomes in mammalian cells," Proc. Natl. Acad. Sci. U.S.A. **84**, 3264–3268 (1987).
[51]G. Lametschwandtner, C. Brocard, M. Fransen, P. Van Veldhoven, J. Berger, and A. Hartig, "The difference in recognition of terminal tripeptides as peroxisomal targeting signal 1 between yeast and human is due to different affinities of their receptor Pex5p to the cognate signal and to residues adjacent to it," J. Biol. Chem. **273**, 33635–33643 (1998).
[52]M. Schrader and H. D. Fahimi, "The peroxisome: still a mysterious organelle," Histochem. Cell Biol. **129**, 421–440 (2008).
[53]F. Fan and K. V. Wood, "Bioluminescent assays for high-throughput screening," Assay Drug Dev. Technol. **5**, 127–136 (2007).
[54]T. F. Massoud, R. Paulmurugan, A. De, P. Ray, and S. S. Gambhir, "Reporter gene imaging of protein-protein interactions in living subjects," Curr. Opin. Biotechnol. **18**, 31–37 (2007).
[55]A. Lundin, "Optimization of the firefly luciferase reaction for analytical purposes," Adv. Biochem. Eng. Biotechnol. **145**, 31–62 (2014).
[56]E. Conti, L. F. Lloyd, J. Akins, N. P. Franks, and P. Brick, "Crystallization and preliminary diffraction studies of firefly luciferase from *Photinus pyralis*," Acta Crystallogr., Sect. D: Biol. Crystallogr. **52**, 876–878 (1996).
[57]D. S. Auld, S. Lovell, N. Thorne, W. A. Lea, D. J. Maloney, M. Shen, G. Rai, K. P. Battaile, C. J. Thomas, A. Simeonov, R. P. Hanzlik, and J. Inglese, "Molecular basis for the high-affinity binding and stabilization of firefly luciferase by PTC124," Proc. Natl. Acad. Sci. U.S.A. **107**, 4878–4883 (2010).
[58]K. Anduleit, G. Sutton, J. M. Diprose, P. P. Mertens, J. M. Grimes, and D. I. Stuart, "Crystal lattice as biological phenotype for insect viruses," Protein Sci. **14**, 2741–2743 (2005).
[59]H. Wang, E. Wei, A. D. Quiroga, X. Sun, N. Touret, and R. Lehner, "Altered lipid droplet dynamics in hepatocytes lacking triacylglycerol hydrolase expression," Mol. Biol. Cell **21**, 1991–2000 (2010).
[60]See supplementary material at http://dx.doi.org/10.1063/1.4921591 for localization data of *in vivo* firefly luciferase crystals (see Fig. S1), images of virus-free vs. baculovirus induced *in vivo* crystallization of luciferase (see Fig. S2), images and movie of bioluminescence induced by enzymatically active soluble firefly luciferase within living cells (see Fig. S3 and movie S3), images of GFP-μNS and luciferase crystals grown within the same cell (see Fig. S4), and the stability analysis of isolated GFP-μNS crystals preliminary to x-ray diffraction experiments (see Fig. S5).
[61]T. Ohkawa, L. E. Volkman, and M. D. Welch, "Actin-based motility drives baculovirus transit to the nucleus and cell surface," J. Cell Biol. **190**, 187–195 (2010).
[62]J. C. Spence, "Approaches to time-resolved diffraction using an XFEL," Faraday Discuss. **171**, 429–438 (2014).
[63]R. Neutze and K. Moffat, "Time-resolved structural studies at synchrotrons and X-ray free electron lasers: Opportunities and challenges," Curr. Opin. Struct. Biol. **22**, 651–659 (2012).
[64]H. Mori, R. Ito, H. Nakazawa, M. Sumida, F. Matsubara, and Y. Minobe, "Expression of *Bombyx mori* cytoplasmic polyhedrosis virus polyhedrin in insect cells by using a baculovirus expression vector, and its assembly into polyhedra," J. Gen. Virol. **74**, 99–102 (1993).
[65]F. Stellato, D. Oberthür, M. Liang, R. Bean, C. Gati, O. Yefanov, A. Barty, A. Burkhardt, P. Fischer, L. Galli, R. A. Kirian, J. Meyer, S. Panneerselvam, C. H. Yoon, F. Chervinskii, E. Speller, T. A. White, C. Betzel, A. Meents, and H. N. Chapman, "Room-temperature macromolecular serial crystallography using synchrotron radiation," IUCrJ **1**, 204–212 (2014).
[66]M. S. Hunter, B. Segelke, M. Messerschmidt, G. J. Williams, N. A. Zatsepin, A. Barty, W. H. Benner, D. B. Carlson, M. Coleman, A. Graf, S. P. Hau-Riege, T. Pardini, M. M. Seibert, J. Evans, S. Boutet, and M. Frank, "Fixed-target protein serial microcrystallography with an x-ray free electron laser," Sci. Rep. **4**, 6026 (2014).